URSI GASS 2020, Rome, Italy, 29 August - 5 September 2020

RADAR Studies of Planetary Surfaces Using Spacecraft Telecommunication Signals: A perspective on evolving methods and technologies.

G.G. Peytaví*(1), T.P. Andert(1), B. Häusler(1), S. Tellmann(2), and M. Pätzold(2)
(1) Institute of Space Technology, Bundeswehr University Munich, 85577 Neubiberg, Germany, https://www.unibw.de/lrt9, graciela.gonzalez@unibw.de
(2) Institute of Planetary Research, Universität zu Köln, 50923 Cologne, Germany

Abstract

Building upon the experiences with bistatic RADAR experiments of opportunity in planetary research, we discuss technologies and methods involved in the implementation, planning, receiver technology and signal processing aspects of these experiments. We highlight relevant technology shifts withch may enable a new generation of RADAR experiments from small platforms.

1 Introduction

Spacecraft telecommunication signals have been successfully exploited for scientific experimentation since the very early days of planetary exploration [1, 2, 3, 4]. In these Radio-Science (RS) experiments, variations in the propagation path of the radio signal are monitored. The radio-frequency bands allocated for deep space communications - S, X and Ka bands - allow radio scientists to observe planetary environments at centimetre wavelengths. A first demonstration of an inter-satellite RS experiment was recently performed at Mars using UHF proximity transponders [10]. Similar experiments at UHF have been proposed [11], showing that the decimetre band is receiving an increasing interest by radio scientists.

By means of an adequate channel model, residual propagation effects (i.e., frequency shifts, phase rotations or depolarization coefficients) have been studied to provide insight into a body's gravitational potential [5], the structure of neutral atmospheres and ionospheres [6, 7], the activity of the solar corona [8], and the RADAR reflectivity of planetary surfaces [9]. Such RS experiments have been conducted at several bodies in our solar system using merely Signals of Opportunity (SO) of high phase stability. In particular, the unmodulated carrier wave of the spacecraft's nominal telecommunication subsystem.

From the observations modes listed above, perhaps one of the less known is that of probing the very top layer of planetary surfaces. In such RADAR experiments, the unmodulated carrier signal is broadcast towards the planetary surface in a favourable incidence geometry intended to produce a quasi-specular reflection. The scattered wave is recorded in a polarimetric RADAR receiver where coherent I-Q demodulator outputs are simultaneously sampled at high-rate (typically 1-25 Kilosamples per second). Such experiments aim at characterizing (1) the electrical properties of the surface from depolarization measures (typically only a subset of the Stokes coefficients) and (2) its cm-scale roughness from the Doppler frequency spread. Through adequate modelling, further constraints on material composition and porosity may be derived, yielding cues about the processes involved in the formation and evolution of the observed surface.

Microwave RADAR probing using telecom SOs has been often conducted from an orbiting platform and mostly, with few exceptions, using a non-collocated transmitter and receiver. Therefore, in the literature we mainly encounter reports about bistatic RADAR studies (cf. [9]). Here onwards we adopt the term SO-RADAR to refer to these experiments, whether monostatic, bistatic or multistatic. These experiments should be well distinguished from specifically designed RADAR instruments.

In this paper, we review the operation modi of SO-RADAR experiments in planetary research leading up to those carried out by Rosetta/RSI at comet 67P/C-G in 2014 [16]. Our focus is set on the technologies and methods involved in the implementation, planning, signal recording and data processing aspects of these experiments. Building upon state of the art developments, we highlight relevant technology shifts that in the authors' opinion may enable a new generation of SO-RADAR experiments from smaller platforms.

2 Implementation

In the mid-60s, Gunnar Fjeldbo [12] theoretically demonstrated that - by means of the Kirchhoff's approximation and application of geometric optics - it is possible to distinguish a direct signal from a spacecraft in planetary opposition from a signal reflected at the planetary surface. Fjeldbo further showed how time-varying statistical properties of the reflected signal could be related to statistical properties of the surface such as: roughness, autocorrelation length or mean dielectric constant. This work was further ex-

tended by several authors well into the 80s. Thereafter various orbital experiments were successfully conducted from spacecraft around the Moon [1, 2], Venus [3, 4], Saturn's moon Titan [13], Mars [14, 9] and Pluto [15]. Most recently, bistatic RADAR experiments were conducted at two smaller bodies, namely comet 67P/C-G [16, 17, 18] and asteroid Vesta [19].

With the exception of the uplink experiments by New Horizons at Pluto [15], all other experiments where conducted in downlink configuration, as depicted in Figure 1. The downlink experiments conducted by Dawn at Vesta were however performed at grazing incidence, hence no polarimetric data could be collected. Instead, the relative reflectivity from site to site could be assessed [19].

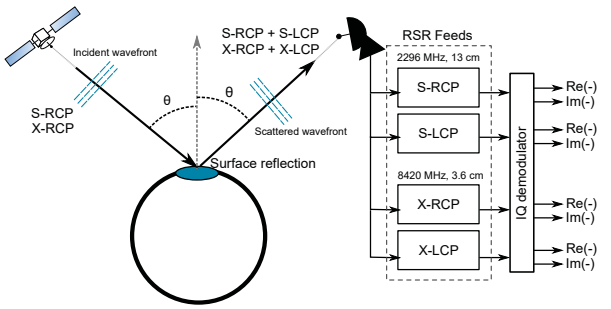

Figure 1. Schematic of a dual-frequency SO-RADAR experiment in downlink configuration. A quasi-specular reflection geometry is depicted, meaning that incident and scattered wavefronts are coplanar with an almost identical angular offset from the local normal at the reflection point.

During a SO-RADAR experiment, the spacecraft on-board communication systems is commanded to transmit a non-modulated carrier signal towards a pre-planned region on the target's surface. For some missions, as it was the case of Rosetta, the High-Gain Antenna (HGA) can be steered for this purpose. Otherwise, a spacecraft attitude mode needs to be developed for the specular pointing sequences. In order to minimise power losses in dichroic reflectors and avoid fading along the propagation path, the transmitted wave is circularly polarized for all deep-space communication transponders. In Figure 1, our sample transmitter broadcasts a dual-frequency (X- and S-band) Right-handed Circularly Polarized (RCP) wave.

A receiving station on Earth, typically a 70-m DSN facility, is operated such that the antenna is pointed at planetary coordinates throughout the surface observations. Two reception channels are operated per frequency band, such that both RCP and Left-handed Circular Polarization (LCP) components of the scattered wave can be recorded. The local oscillator of the receiving station is tuned to the Doppler shift predicts of the transmitting spacecraft, such that the direct signal component is present within the reception bandwidth. For each channel, an in-phase and quadrature (IQ) demodulator is available, such that amplitude and phase of each polarization component can be recovered. Note that in order to combine the different channels, an amplitude and phase calibration procedure is required. Typically a relative calibration procedure between channels is recommended [9].

The collected data consists of non-calibrated complex voltage samples. At DSN facilities, this open-loop recording mode is performed at 1-100 Ksamples/sec and most commonly at 25 Ksamples/sec.

For weak and spectrally adjacent SO-RADAR echoes, the phase stability of the local oscillator at the transmitter is paramount to enable a sufficiently long signal integration window, such that the echo and direct signals may be discriminated in post-processing.

3 Experiment Planning

In a classic downlink SO-RADAR implementation, an attitude command timeline is uploaded to the spacecraft prior to the experiment. This attitude timeline aims at steering the main beam of the High-gain Antenna (HGA) towards the specular reflection point (SP) during the 1-5 hours observation sequence. The length of the observation ultimately depends on the spacecraft-body-Earth relative dynamics.

At large bodies like e.g. Mars, the specular pointing sequence can be computed accurately assuming an spheroidal model of the body. First, observation windows targeting the planetary limb should be identified. These can be found in near occultation geometry. The search algorithm should then check for the co-planarity - i.e., $\theta_a = \mathbf{n} \cdot (\mathbf{k}_i \times \mathbf{k}_r) = 0$ - of the spacecraft-SP $\mathbf{k}_i$ unit vector, the SP-Earth $\mathbf{k}_r$ unit vector and the local normal $\mathbf{n}$ in a common reference frame, e.g. a body-centered J2000 realization. The local surface normal can be derived from the shape model. The same vectors lead to an estimate of the specular reflection angle $\theta = \theta_i = \theta_r = \arccos(\mathbf{k}_i \cdot \mathbf{n}) = \arccos(\mathbf{k}_r \cdot \mathbf{n})$.

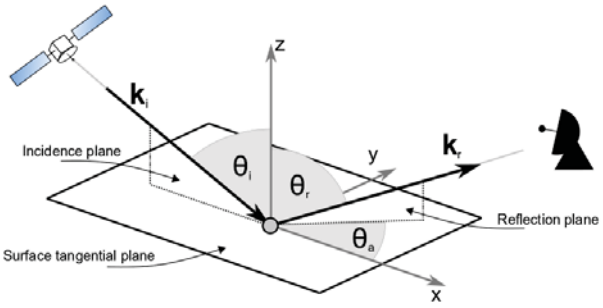

Figure 2. Schematic of out-of-plane reflection geometry.

Considering the Fresnel amplitude reflection coefficients for linear horizontal R_H and linear R_V polarizations (eq. 1-2), the power reflection coefficients for same-sense ρ_{SC} and opposite-sense ρ_{OC} polarizations can be found as linear combination of the previous (eq. 3-4).

$$R_H = \frac{\cos(\theta) - \sqrt{\varepsilon - \sin^2\theta}}{\cos(\theta) + \sqrt{\varepsilon - \sin^2\theta}} \quad (1)$$

$$R_V = \frac{\varepsilon\cos(\theta) - \sqrt{\varepsilon - \sin^2\theta}}{\varepsilon\cos(\theta) + \sqrt{\varepsilon - \sin^2\theta}} \quad (2)$$

$$\rho_{SC} = \frac{|R_H + R_V|^2}{4} \quad (3)$$

$$\rho_{OC} = \frac{|R_H + R_V|^2}{4} \quad (4)$$

Typically, the experiment scheduler would prioritize observations providing similar power returns in opposite-sense polarizations $\rho_{SC}/\rho_{OC} \approx 1$. This selection criteria requires an adequate assumption on the expected mean permittivity ε of the surface. This selection reduces the need for an absolute amplitude calibration of the data [9].

For small irregular bodies, the planning of a specular sequence is a non-trivial task. The best available shape model must be exploited to identify orbit arcs with the most favourable geometry, slow dynamics, reduced clutter and no blockage. Figure 3 is an example of the geometry analysis for the footprint of Rosetta/RSI HGA on the surface of comet 67P/C-G.

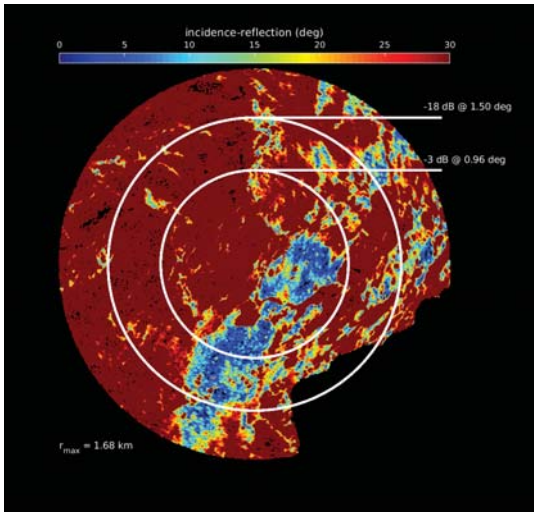

Figure 3. Example of a SO-RADAR geometry analysis for the footprint of Rosetta/RSI HGA on a detailed shape model of comet 67P/C-G. Depicted are surface facets of approx. 30 cm edge-length. Color coding indicates quasi-specular regions (blue) and non-specular regions (red). Concentric white circles mark the half-power beam width and first side lobe peak of the antenna, respectively.

4 Detectability: The Bistatic RADAR Equation and Forward Modelling

Let us consider a transmitter system on the spacecraft with available power P_t and antenna gain G_t. The transmitter is located at a distance $|\mathbf{r}_t|$ from the specular point on the target's surface. Let us also consider a receiver system located at a distance $|\mathbf{r}_r|$ from the specular point. The receiver sensing aperture is of effective size A_r meters. The effectively received power dP_r from a surface element dS accounting for spheric wave propagation (i.e., free-space loss) is a function of the surface normalized radar cross-section σ_0, as provided in eq. 5. The radar cross-section is a measure of the surface capability to reflect microwave radiation. This measure is dependant on viewing geometry and material properties, hence $\sigma_0 = \sigma_0(\theta, \varepsilon)$.

$$dP_r = \frac{P_t G_t}{4\pi|\mathbf{r}_t|^2}\sigma_0\frac{A_r}{4\pi|\mathbf{r}_r|^2}dS \quad (5)$$

In order to assess the sensitivity of our receiver system to echoed signals from the surface of a target we are required to integrate the expression in eq. 5 over the effective scattering area for the predicted geometry. Traditionally, an statistical representation of the surface is adopted, such that a close-form analytical expression of the radar cross-section can be derived. Hagfors' assumption of a surface with Gaussian height distribution and exponential correlation function has been often adopted [14, 9]. This assumption is consistent with results obtained for fractal surface representations with Brownian motion [9].

With state of the art computing power, numerical alternatives are now available to assess detectability. Given a realistic facet shape model of a target, material properties can be assigned to individual facets creating 2-D or 3-D meshes over which a numerical electromagnetic solver can be applied (See Figure 4). This procedures allows for a flexible assessment of detectability boundaries for different surface composition and porosity.

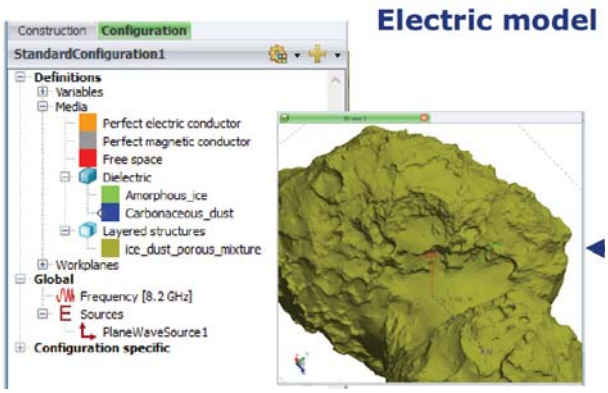

Figure 4. Screenshot of the electric model configuration window of the FEKO electromagnetic solver by Altair Hyperworks.

5 Receiver Technology and Signal Processing

SO-RADAR signal reception is performed using open-loop architectures. In these systems, the phase and frequency

tracking loops are not fed a correction between the incoming signal and the local generated replicas, but rather a preloaded forecast of these values. In addition, these system execute a high-rate sampling of the receiver bandwidth providing a quasi-instantaneous snapshot of the spectra.

State-of-the-art spacecraft communication system are not specifically designed as open-loop receivers, as there is no need for a spacecraft to sample the frequency spectrum since telecommunication frequency allocations are fixed in the S-, X- and Ka-bands. This is the reason for most SO-RADAR experiments to be conducted in downlink configuration. For UHF proximity transponders such as JPL's Electra and KinetiQ's Melacom, a larger spectral flexibility is available to account for larger Doppler frequency shifts during entry, descent and landing operations. This ability of the transponders could be well exploited for SO-RADAR signal recording, although with limited encoding resolution.

The next generation of RF spacecraft receivers, specially for small platforms with technology demonstration capability, may well see the introduction of software-defined radio architectures where the Analog-to-Digital converters are shifted further upfront into the RF front-end. This modification will require the integration of high-rate sampling devices and more powerful computational units - such as Graphics Processing Units (GPUs) - able to deal with high data throughout in reception. Such system should be able to compute a real-time spectrogram as depicted in Figure 5, identify areas of high-information content and store a sufficiently decimated version of these data fragments into memory.

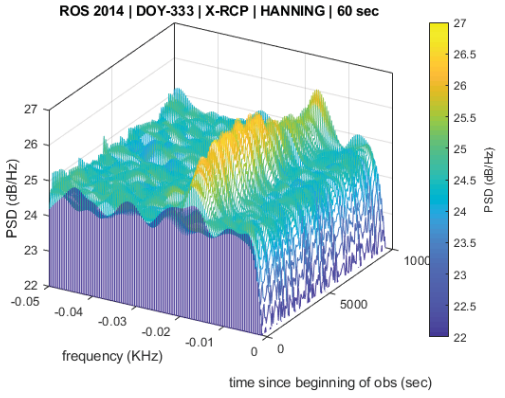

Figure 5. Sample spectrogram from Rosetta/RSI bistatic RADAR observations at comet 67P/C-G

Such system will require good phase stability to perform these tasks, in particular when performing experiments in low dynamic environments such as in proximity of small bodies. In these scenarios, the direct signal and the surface echo may appear adjacent in frequency within a few Hertz (See Figure 6). Long signal integration intervals may be required to identified the echo in these cases, and this is only possible is phase stability is guaranteed over the integration interval. Chip-scale atomic clocks with phase stability of 10^{-10} to 10^{-11} parts (Allan deviation) over 10-100 seconds are already available in the market, and much development is expected in this area in the next couple of years.

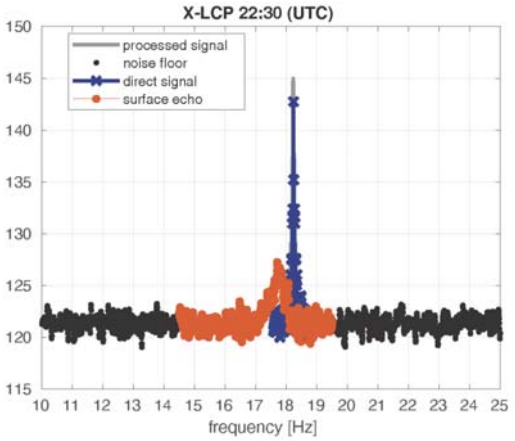

Figure 6. Uncalibrated spectra of the X-LCP records collected by Rosetta/RSI during a bistatic RADAR experiment at comet 67P/C-G. The spectrally adjacent direct (blue) and echo (orange) signals have be identified and classified over the noise level (black).

Efficient statistical methods for spectral estimation are being developed in the scope of machine learning applications. Line-spectra estimators and model-based estimators can be trained on legacy RADAR data archives. It can be expected that some of these methods will have applicability in the smart data handling of future SO-RADAR experiments with application in signal detection, classification, tracking and reduction.

6 A Future Perspective for SO-RADAR Experiments

The capability to operate a bistatic/multistatic experiment with two or more orbiting platforms instead of an Earth-based receiving station would allow for more geometric freedom in the planning of SO-RADAR observations. With a single orbiter the area of coverage as well as the frequency of the observations is limited by the near Earth-occultation geometry. With two orbiters, the frequency of cross-occultation events is significantly larger as has been highlighted for current Mars orbiters [10, 11]. Possible issues may arise regarding pointing accuracy of the smaller, resource-limited platforms. The usage of wide-beam antennae (e.g., patch antennae) with a analog-to-digital converters located directly at the RF front-end - in the fashion of Multiple-Input-Multiple-Output (MIMO) technology - may well be a suitable way to address this issue. The use of less convergent or even lossy antenna can be justified for short links in which the power budget is no longer the limiting feasibility factor. MIMO systems open the door to new concepts such as the application of smart digital beamforming to: specular point tracking, or discriminative echo/direct signal tracking.

References

[1] G.L. Tyler and H.T. Howard, "Dual-Frequency Bistatic-Radar Investigation of the Moon with Apollos 14 and 15," *Journal of Geophysical Research*, Vol. **78**, No. **23**, 1973, pp. 4852–4874.

[2] R. Simpson and G.Tyler, "Radar Scattering Laws for the Lunar Surface," *IEEE Transactions on Antennas and Propagation*, Vol. **30**, No. 2, 1982, pp. 438–449, doi: 10.1109/TAP.1982.1142803

[3] R.A. Simpson, G.L. Tyler, B.Häusler, R. Mattei, and M. Pätzold, "Venus Express bistatic radar: High-elevation anomalous reflectivity," *Journal of Geophysical Research*, Vol. **114**, No. **E9**, June 2009, doi: 10.1029/2008JE003156

[4] G.H. Pettengill, P.G. Ford, R.A. Simpson, "Electrical Properties of the Venus Surface from Bistatic Radar Observations," *Science*, Vol.**272**, No.**5268**, June 1996, pp. 1628–1631, doi: 10.1126/science.272.5268.1628

[5] T.P. Andert, "Masses of Small Bodies,", *Disseration*, 2010, Universität zu Köln, doi: 10.23689/FIDGEO-7

[6] S. Tellmann, M. Pätzold, B. Häusler, D.P. Hinson, and G.L. Tyler, "The structure of Mars lower atmosphere from Mars Express Radio Science (MaRS) occultation measurements," *Journal of Geophysical Research*, Vol. **118**, No. **2**, February 2013, doi: 10.1002/jgre.20058.

[7] M. Pätzold, S. Tellmann, B. Häusler, D. Hinson, R. Schaa, and G.L. Tyler, "A Sporadic Third Layer in the Ionosphere of Mars," *Science*, Vol. **310**, November 2005, doi: 0.1126/science.1117755

[8] M. Pätzold, M.K. Bird, P. Edenhofer, S.W. Asmar and T.P. McElrath, "DualâĂŘfrequency radio sounding of the solar corona during the 1995 conjunction of the Ulysses spacecraft," *Geophysical Research Letters*, Vol. **22**, No. **23**, December 1995, doi: 10.1029/95GL03184

[9] R.A. Simpson, G.L. Tyler, M. Patzold, B. Hausler, S.W. Asmar, and A.K. Sultan-Salem, "Polarization in bistatic radar probing of planetary surfaces: Application to mars express data", *Proceedings of the IEEE*, Vol. **99**, No. **5**, 2011, pp. 858–874, doi: 10.1109/JPROC.2011.2106190

[10] S. Asmar, C. Ao, C. Edwards, D. Kahan, X. Pi, M. Paik, and A. Manucci, "Demonstration of Mars crosslink occultation measurements for future small spacecraft constellations,", *IEEE Aerospace Conference*, 2016, doi: 10.1109/AERO.2016.7500729

[11] S. Tellmann, M. Pätzold, B. Häusler, M.K. Bird, D.P. Hinson, T.P. Andert, G.G. Peytaví, and S.W. Asmar, "Crosslink Occultations for probing the planetary atmosphere and ionosphere of Mar," *EPSC-DPS Joint Meeting 2019*, Vol. **13**, September 2019

[12] Gunnar Fjeldbo, "Bistatic-Radar Methods for Studying Planetary Ionospheres and Surfaces," *Final Report* Prepared under National Science Foundation Grant NsF G-21543 and *Scientific Report*, No. **2** Prepared under National Aeronautics And Space Administration Research Grant No. NsG-377, April 1964, pp. 64–81. Radioscience Laboratory, Stanford University.

[13] M. Pérez - Ayúcar, R. D. Lorenz, N. Floury, R. Prieto-Cerdeira, and J.-P. Lebreton, "Bistatic observations of Titan's surface with the Huygens probe radio signal," *Journal of Geophysical Research*, Vol. **111**, No.**E7**, July 2006, doi: 10.1029/2005JE002613

[14] R.A. Simpson, "Spacecraft Studies of Planetary Surfaces Using Bistatic Radar," *IEEE Transactions on Geoscience and Remote Sensing*, Vol. **31**, No. **2**, March 1993.

[15] I. Linscott et al., "Pluto's Surface Properties from the New Horizons Uplink Bistatic Radar Experiment," Invited Poster at *AGU Fall Meeting 2009*, December 2009.

[16] M. Pätzold et al., "Rosetta Radio Science Investigations (RSI)," *Space Sci Rev*, Vol.**128**, pp. 599–627, 2007, doi: 10.1007/s11214-006-9117-7

[17] T.P. Andert et al., "First Rosetta Radio Science Bistatic Radar Observations of 67P/Churyumov-Gerasimenko," *EGU General Assembly 2015*, Vol. **17**, 2015.

[18] G.G. Peytaví, T.P. Andert, M. Pätzold, B. Häusler, S. Remus, S. Tellmann, M.K. Bird, S.W. Asmar, "Processing Bistatic Radar Observations of Comet 67P/C-G by the RSI Experiment aboard Rosetta,", *AGU Fall Meeting 2018*, December 2018.

[19] E.M. Palmer, E. Heggy, and W. Kofman,"Orbital bistatic radar observations of asteroid Vesta by the Dawn mission," *Nature Communications*, Vol.**8**, No.**1**, 2017, doi: 10.1038/s41467-017-00434-6